Journal of Magnetism and Magnetic Materials 342 (2013) 100–107

Contents lists available at SciVerse ScienceDirect

Journal of Magnetism and Magnetic Materials

journal homepage: www.elsevier.com/locate/jmmm

Suppression of the long-range magnetic order in $Pb_3(Mn_{1-x}Fe_x)_7O_{15}$ upon substitution of Fe for Mn

N.V. Volkov [a], E.V. Eremin [a,*], O.A. Bayukov [a], K.A. Sablina [a], L.A. Solov'ev [b], D.A. Velikanov [a], N.V. Mikhashenok [a], E.I. Osetrov [a], J. Schefer [c], L. Keller [c], M. Boehm [d]

[a] Kirensky Institute of Physics, Russian Academy of Sciences, Siberian Branch, Krasnoyarsk 660036, Russia
[b] Institute of Chemistry and Chemical Technology, Russian Academy of Sciences, Siberian Branch, Krasnoyarsk 660049, Russia
[c] Laboratory for Neutron Scattering, ETH Zurich and Paul Scherrer Institut, CH-5232 Villigen PSI, Switzerland
[d] Institut Laue-Langevin, 6 rue Jules Horowitz, BP 156, 38042 Grenoble, Cedex 9, France

ARTICLE INFO

Article history:
Received 9 October 2012
Received in revised form
12 April 2013
Available online 25 April 2013

Keywords:
Crystal growth
Ferrimagnetism
Layered magnetic compounds

ABSTRACT

Structure and magnetic properties of $Pb_3(Mn_{1-x}Fe_x)_7O_{15}$ single crystals with $x=0$–0.2 grown by spontaneous crystallization from solution in melt have been investigated. All the crystals belong to the hexagonal space group $P6_3/mcm$. The magnetic properties appeared to be strongly dependent on the iron doping level. At small ($x=0.05$) dopant concentrations, the value of magnetization and Neel temperature T_N decrease insignificantly ($T_N=70$ K). With increasing x, the three-dimensional magnetic ordering does not occur and temperature dependences of magnetization at $x\geq0.1$ exhibit spin-glass-like features in the low-temperature region.

1. Introduction

Manganites with mixed-valence of manganese are oxide compounds that have been attractive objects of investigation for the last few decades. Rich variety of their physical properties caused by the interplay of charge, spin, and orbital degrees of freedom and possibility of controlling these properties make these materials interesting for both fundamental research and application [1]. The most systematically studied compounds are the manganites with the perovskite structure $R_{1-x}A_xMnO_3$ (R is the rare-earth element and A is Ca, Sr, Ba, Pb, etc.). In the perovskite structure, Mn^{3+} and Mn^{4+} cations are localized in octahedra joint vertices. This circumstance plays a key role in the picture of the exchange interactions. Mixed-valence manganese oxides with the structures different from perovskite one remain understudied; however, a number of recent studies have been devoted to the materials (for instance, $Pb_3Mn_5V_2O_{16}$ [2] and $BaMn_3O_6$ [3]) where oxygen octahedra have, as a rule, common edges and form single layers. Being still not clearly understood, various intriguing physical phenomena observed in the doped perovskite-like manganites stimulate the search for other oxide families containing mixed-valence manganese ions with the structure different from the perovskite one.

Of particular interest is the natural mineral zenzenite with the chemical formula $Pb_3(Fe^{3+}Mn^{3+})_4Mn_3^{4+}O_{15}$ where Mn^{3+} ions are partially replaced by Fe^{3+} ions. Despite the artificial zenzenite was grown long ago [4], its physical properties have not been studied. There is a known work of Bush et al. [5] devoted to the investigation of magnetic and electrical properties of the crystal with the chemical formula $Pb_3Mn_6O_{13}$. In our previous studies, we reported data on the magnetic [6], dielectric [7], and calorimetric [8] properties of the $Pb_3Mn_7O_{15}$ single crystals with mixed-valence manganese ions. We found anomalies on the temperature dependence of magnetization at $T_1=160$ K, $T_2=70$ K, and $T_3=25$ K, which were consistent with the anomalies on the temperature dependence of specific heat. The temperature dependences of ε' and ε'' also exhibit anomalies in the temperature range 150–210 K that strongly depend on frequency. The most important questions unanswered by now are where the magnetic phase transitions originate from and how they transform the magnetic structure. There still has been a lack of unified interpretation of anomalies on the temperature dependence of complex permittivity. It is unclear whether there are charge ordering and small-radius polarons and, if there are, whether they are evoked by the stereoactivity of Pb^{2+} ions.

The crystal structure of $Pb_3Mn_7O_{15}$ was described first by Darriet et al. [9] on the basis of the orthorhombic $Cmc2_1$ space group. Later, Marsh and Herbstein. [10] reconsidered the structure

* Correspondence to: Kirensky Institute of Physics, SB RAS, Akademgorodok 50, Building 38, Krasnoyarsk 660036, Russia. Tel.: +7 391 2432635; fax: +7 391 2438923.
E-mail address: eev@iph.krasn.ru (E.V. Eremin).

0304-8853/$ - see front matter © 2013 Elsevier B.V. All rights reserved.
http://dx.doi.org/10.1016/j.jmmm.2013.04.054

in the space group *Cmcm* using the single-crystal data of Darriet et al. [9]. Then, Le Page and Calvert [11] proposed the hexagonal unit cell with the space group $P6_3/mcm$. In Holstman's et al. work [4], zenzenite $Pb_3(Fe^{3+}Mn^{3+})_4Mn_3^{4+}O_{15}$ also has the hexagonal $P6_3/mcm$ symmetry. According to the data of our preliminary X-ray diffraction (XRD) measurements on powders prepared by grinding of $Pb_3Mn_7O_{15}$ single crystals, most of the observed XRD peaks can be satisfactorily indexed in the hexagonal space group $P6_3/mcm$ at room temperature [6]. Recently, we carried out additional structural studies on a high-resolution synchrotron in the temperature range 15–295 K [12]. The results appeared surprising: the obtained orthorhombic structure with the space group *Pnma* was not found in the previous studies on $Pb_3Mn_7O_{15}$ [4,6,9–11]. The thermogravimetric analysis allowed us to determine the oxygen content $x=14.93\pm0.05$ in the samples [12]. No structural phase transitions were observed within the investigated temperature range 15–300 K [12]. As we discovered later, upon heating $Pb_3Mn_7O_{15}$, the room-temperature orthorhombic *Pnma* structure transformed first (at $T_1=400$ K) to a spatially modulated structure and then (at $T_2=560$ K), to the hexagonal $P6_3/mcm$ structure [13].

These contradictory structural data might originate from an enhanced sensitivity of the $Pb_3Mn_7O_{15}$ structure to the crystal growth conditions or deviations in the synthesis parameters, almost unavoidable at repeatable synthesis. Another possible explanation might be the influence of impurity traces in initial chemical reagents. We grew the crystals with different dopants (Li, Ga, Ge, Ru, etc.) in small concentrations (~5 at%) and found that small amounts of impurities embedded in $Pb_3Mn_7O_{15}$ did not affect its crystal structure. In some samples with impurities, the Neel temperature dropped from 70 to 65 K, which was apparently related simply to the diamagnetic dilution [13]. Doping of $Pb_3Mn_7O_{15}$ with 3-d and 4-d ions in amounts of ~10–30 at% led to the noticeable changes in the structure and magnetic properties, as was shown for $Pb_3Mn_{5.5}Ni_{1.5}O_{15}$ [14].

In this study, we systematically investigate the effect of substitution of iron for manganese on the magnetic and structural properties of the $Pb_3(Mn_{1-x}Fe_x)_7O_{15}$ single crystals. The choice of iron as a substitute was imposed by the following circumstances. According to the results of the recent studies on the effect of Fe substitution on the magnetic and transport properties of manganites with the general formula La(Sr, Pb)$(Mn_{1-x}Fe_x)O_3$ [15,16], in these compounds iron ions are always in the high-spin $3t_{2g}2e_g$ state. The authors of the mentioned works followed variations in the magnetic properties of the crystals with the change in the Mn^{3+}/Mn^{4+} ratio. We assume that embedding of Fe^{3+} in our compound can also change the Mn^{3+}/Mn^{4+} ratio. In order to identify the positions, valences, and electron states of iron ions, we performed XRD and Mossbauer studies on our samples with embedded Fe^{57}. Despite the ionic radii of Mn^{3+} and Fe^{3+} are close, the octahedra occupied by the Jan–Teller Mn^{3+} ions upon their replacement by Fe^{3+} will become less distorted. Will this affect the structural and magnetic properties of $Pb_3Mn_7O_{15}$? Here, we attempt to answer this question.

2. Experimental details

2.1. Sample preparation

Single crystals of $Pb_3(Mn_{1-x}Fe_x)_7O_{15}$ manganites with $x=0$, 0.05, 0.1, 0.15, and 0.2 were grown by a flux method. As a flux, PbO was chosen, known as an effective solvent for many oxide compounds and preventing incorporation of foreign ions into the lattice. The synthesis was started with heating the mixture of appropriate amounts of high purity PbO, Mn_2O_3, and Fe_2O_3 in a platinum crucible at 1000 °C for 4 h. Then, the crucible was slowly cooled down to 900° with the rate $v=2$–5 °/h and, finally, the furnace was cooled to room temperature. Single crystals of a plate-hexagonal shape with black shiny facets were found at the solidified liquid surface. The plates were up to 40 mm in "diameter". The grown crystals were mechanically extracted from the flux. The magnetic measurements reported in this study were performed on well-polished plate-like samples of the required dimension that were cut from the resulting single-crystal plates. The samples were oriented by the back-Laue method.

2.2. Measurements

Powder X-ray diffraction (PXRD) data were collected on a PANalytical X'Pert PRO diffractometer equipped with a solid state detector PIXcel and a secondary graphite monochromator. To ensure the reproducibility of the analysis, two powder samples of the material were prepared. The samples were ground in an agate mortar with octane and further annealed at 1073 K to reduce microstrains. The full-profile crystal structure analysis was made by applying the Rietveld formalism [17] and the derivative difference minimization (DDM) [18] refinement method. In the full-profile refinement, the effects of preferred orientation, anisotropic broadening, and surface roughness were taken into account.

Mossbauer measurements were performed with an EM1104Mc spectrometer at room temperature with a $Co^{57}(Cr)$ source on powders obtained from single crystals doped with iron enriched with a Fe^{57} isotope by 86%. The doping levels of $Pb_3(Mn_{1-x}Fe_x)_7O_{15}$ were $x=0.05$ and $x=0.15$. The X-ray and Mossbauer measurements confirmed that iron ions are almost completely embedded in the crystal matrix. The Mossbauer spectra were identified in two stages. At the first stage, the probability distributions of quadrupole splittings P(OS) in the experimental spectrum were determined with fitting of the isomeric chemical shift common for the entire doublet group. The features in the P(OS) indicate possibly nonequivalent positions. This information was used in constructing the model spectrum. At the second identification stage, this spectrum was fit to the experimental spectrum by varying the entire set of superfine parameters. During the fitting, the exact Mossbauer parameters of nonequivalent positions were determined. False features arising due to the use of the common chemical shift for the spectra set were nullified.

The magnetic properties of the crystals were studied using dc magnetization measurements on a Physical Property Measurement System (PPMS, Quantum Design) at temperatures from 2 to 300 K in magnetic fields up to 90 kOe.

3. Result and discussion

3.1. Structural properties

Preliminary analysis of the PXRD data showed that all the $Pb_3(Mn_{1-x}Fe_x)_7O_{15}$ crystals with $x=0.05$, 0.1, 0.15, and 0.2 were isostructural to zenzenite [12] and the high-temperature phase of $Pb_3Mn_7O_{15}$ [14]. The structure of the crystals is characterized by the hexagonal $P6_3/mcm$ unit cell with four sites of Mn atoms: Mn1 (12i), Mn2(8h), Mn3(6f), and Mn4(2d).

To analyze the distribution of Fe over Mn-related sites, we performed the PXRD measurements for $Pb_3(Mn_{1-x}Fe_x)_7O_{15}$ with $x=0.15$ using both Cu Kα and Co Kα radiations, for which Mn and Fe atoms have noticeably different anomalous dispersion coefficients. The structure refinement for the two prepared samples at two different wavelengths was performed first with a model containing only Mn atoms in the corresponding sites. The distinction in the anomalous dispersion properties of Fe and Mn manifested itself in systematic differences of the refined isotropic displacement parameters (U_{iso}) of the Mn-sites obtained from Cu

Kα and Co Kα data. The values of these differences normalized to their estimated standard uncertainties (e.s.u.) are plotted for all the 10 atoms of the structure in Fig. 1. The largest positive differences were reproducibly observed for sites Mn2(8h) and Mn3(6f), suggesting that the Fe atoms were localized mainly in these sites.

To finally refine the structure, we merged the PXRD patterns for the two samples and included Fe atoms in the model. The refinement was made for both Cu Kα and Co Kα data. The occupancy fractions of Fe atoms were chosen such that the differences in the refined U_{iso} parameters for the Mn-related sites were minimum. The results are summarized in Table 1. The method described above yielded an estimated total Fe content in the structure of 16.5 at%, which is close to 15 at% introduced in the synthesis.

3.2. Mossbauer properties

Mossbauer spectra of $Pb_3(Mn_{1-x}Fe_x)_7O_{15}$ with $x=0.05$ and 0.15 represent nonsymmetrical quadrupole doublets (Fig. 2). Processing of the spectra by two singlets shows that the left lines of the spectra are noticeably wider than the right ones: 0.38 mm/s against 0.33 mm/s for the sample with $x=0.05$ and 0.43 mm/s against 0.39 mm/s for the sample with $x=0.15$. The difference in the doublet linewidths indicates that the nonsymmetrical character of the doublet is related not to the Gol'danskii–Karyagin effect but to the presence of several nonequivalent positions of iron. To determine a number of possible nonequivalent positions in the material, the distribution of probability of quadrupole splittings (QS) in the experimental spectrum P(QS) was built (Fig. 3). In determining P(QS), the isomer chemical shift (IS) common for the entire doublet group was fit.

It can be seen from Fig. 3 that the P(QS) distribution has two features for the composition with $x=0.05$ and three features for the composition with $x=0.15$. They are indicated by arrows in the Fig. 3. The number of the features points out the number of possible nonequivalent positions of iron in the material. Based on these data, we built model spectra and fit them to those obtained

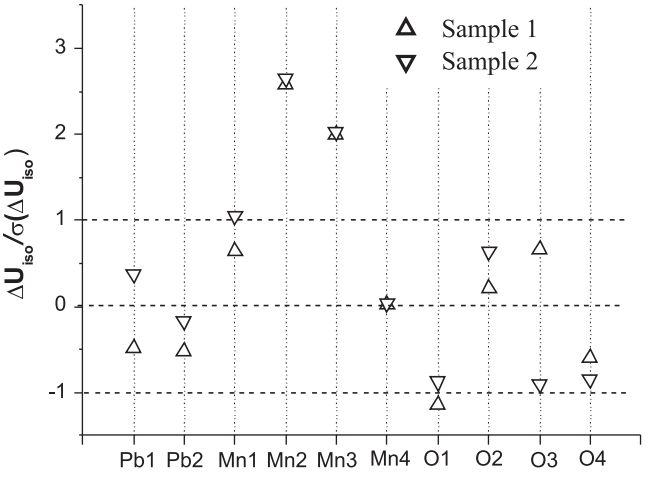

Fig. 1. Values of e.s.u.-normalized difference $\Delta U_{iso}/\sigma(\Delta U_{iso})$. between isotropic displacement parameters obtained from structure refinement on Cu Kα and Co Kα data for two $Pb_3(Mn_{0.85}Fe_{0.15})_7O_{15}$ samples.

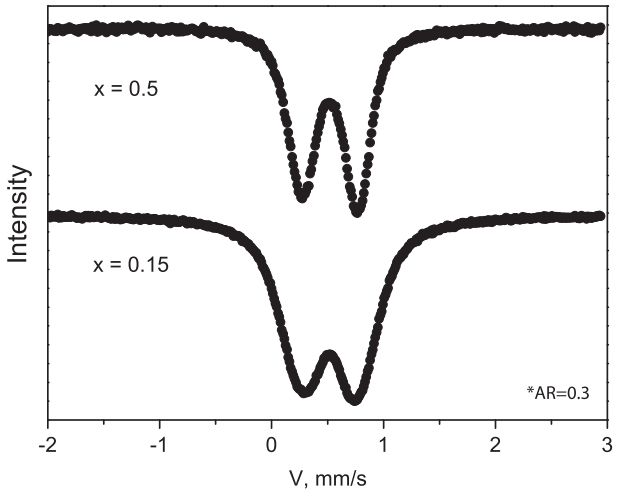

Fig. 2. Mossbauer spectra of $Pb_3(Mn_{1-x}Fe_x)_7O_{15}$ with $x=0.05$ and $x=0.15$ at room temperature.

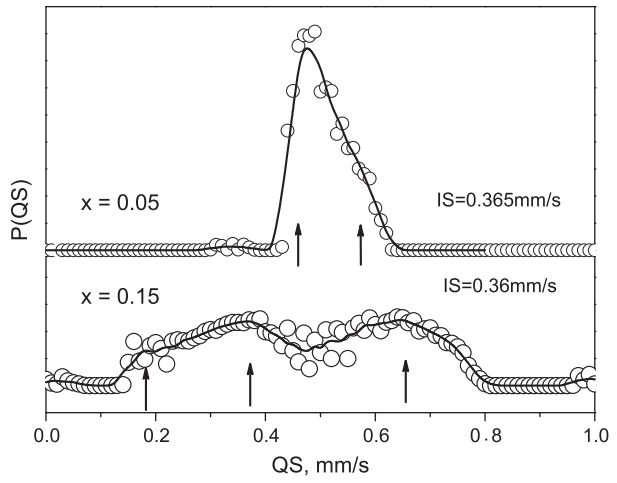

Fig. 3. Distribution of quadrupole splittings (observed—circle, calculated—solid line) in the spectrum of $Pb_3(Mn_{1-x}Fe_x)_7O_{15}$ with $x=0.05$ and $x=0.15$.

Table 1
Experimental conditions and structure refinement results for Cu Kα and Co Kα data.

Structural formula	$Pb_3(Mn_{0.835}Fe_{0.165})_7O_{15}$	
Space group	$P6_3/mcm$	
Radiation	Cu Kα	Co Kα
2Θ range	9–110°	11–144°
Cell parameters	$a=10.0229(2)$ A $c=13.6079(2)$ A	$a=10.0227(2)$ A $c=13.6080(2)$ A
Cell volume	1183.88(5) A^3	1183.84(5) A^3
Z	4	
R-DDM	5.93%	5.65%
R_{Bragg}	2.80%	2.43%

Table 2
Mossbauer parameters of $Pb_3(Mn_{1-x}Fe_x)_7O_{15}$ with $x=0.05$ and $x=0.15$. Column IS is isomer chemical shift, column QS is quadrupole splitting, column W is Mossbauer absorption linewidth, columns A(M.E.) and A(R) are populations of the nonequivalent positions estimated using the Mossbauer technique and determined by the X-ray method.

	IS, mm/s ± 0.005	QS, mm/s ± 0.01	W, mm/s ± 0.01	A(M.E.) ± 0.02	A (R)	Position
$x=0.05$	0.355	0.61	0.21	0.06		Fe2(8h)
	0.371	0.42	0.24	0.15		Fe3(6f)
$x=0.15$	0.378	0.22	0.29	0.06	0.06	Fe1 (12i)
	0.360	0.68	0.37	0.26	0.28	Fe2(8h)
	0.364	0.43	0.31	0.25	0.28	Fe3(6f)

experimentally, varying the entire set of the parameters of the superfine structure. The fitting results are given in Table 2, where the isomer chemical shift is indicated relative to α-Fe and *W* is the Mossbauer absorption linewidth.

The values of the IS indicate that we deal with Fe^{3+} cations occupying sextantal (octahedral) coordination by oxygen. Populations A(M.E.) of the nonequivalent positions for the composition with $x=0.15$ estimated using the Mossbauer technique coincide well with the A(R) populations determined by the X-ray method. This correlation allows identification of the quadrupole doublets observed using the Mossbauer effect.

As can be seen from Table 2, at a low doping level, iron occupies two crystallographic positions, Fe2(8h) and Fe3(6f), preferring the Fe3(6f) positions. With increasing doping level ($x=0.15$), iron starts occupying the third, Fe1(12i) position, preferring the Fe2(8h) and Fe3(6f) positions populated by iron ions already with equal probabilities. Broadening of the quadrupole splitting distribution (Fig. 3) with increasing doping level indicates inhomogeneity of local surroundings of iron positions. This is confirmed by the doublet linewidths (Table 2). An increase in the quadrupole splittings with doping level implies an increase in lattice distortions.

3.3. Magnetic properties

First, let us clarify the terms. The "along-axis" direction implies the direction along the *a* axis for the orthorhombic *Pnma* structure or the direction along the *c* axis of the hexagonal *P6₃/mcm* structure (Fig. 4); the "in-plane" direction is the direction in the *b*–*c* plane for *Pnma* or in the *a*–*b* plane for *P6₃/mcm*.

Fig. 5 shows temperature dependences of magnetization measured on the $Pb_3(Mn_{1-x}Fe_x)_7O_{15}$ single crystals in the "in-plane" magnetic field. For the samples with $x=0$, the low-temperature behavior of magnetization and the isothermal curves up to 80 kOe at different directions of the magnetic field relative to the crystallographic axes were described in detail in our previous work [6]. With decreasing temperature, near $T_1=160$ K, we observe a low, strongly broadened peak (the inset in Fig. 5(a)) on the temperature dependence of magnetization. The nature of this anomaly is not quite clear; it is related, most likely, to the occurrence of cluster ordering. With a further decrease in temperature, at $T_2=70$ K, the long-range magnetic order occurs with a weak spontaneous ferromagnetic moment lying in the crystal plane and related apparently to the noncollinear character of magnetic sublattices. At $T_3=25$ K, there is, probably, a spin-reorientation transition. Doping of $Pb_3Mn_7O_{15}$ by Fe ions in small concentrations ($x=0.05$) leads to the situation when the value of magnetization and Neel temperature T_N decrease insignificantly and the broad peak at $T_1=160$ Kspread more (the inset in Fig. 5(b)). With a further increase in *x*, the form of the magnetization curves drastically changes (Fig. 5 (c–e)): the broad peak at $T_1=160$ K vanishes, the long-range magnetic order does not occur, and the temperature dependences of magnetization for ≥0.1 reveal the spin-glass-like features at low temperatures, with typical divergence of magnetization at different regimes (with and without magnetic field) of sample cooling.

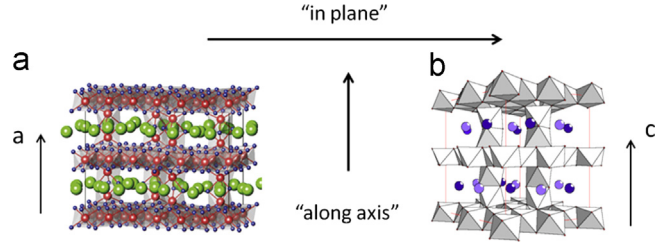

Fig. 4. Unit cells for the orthorhombic *Pnma* [12] (a) and hexagonal *P6₃/mcm* [6] (b) symmetries.

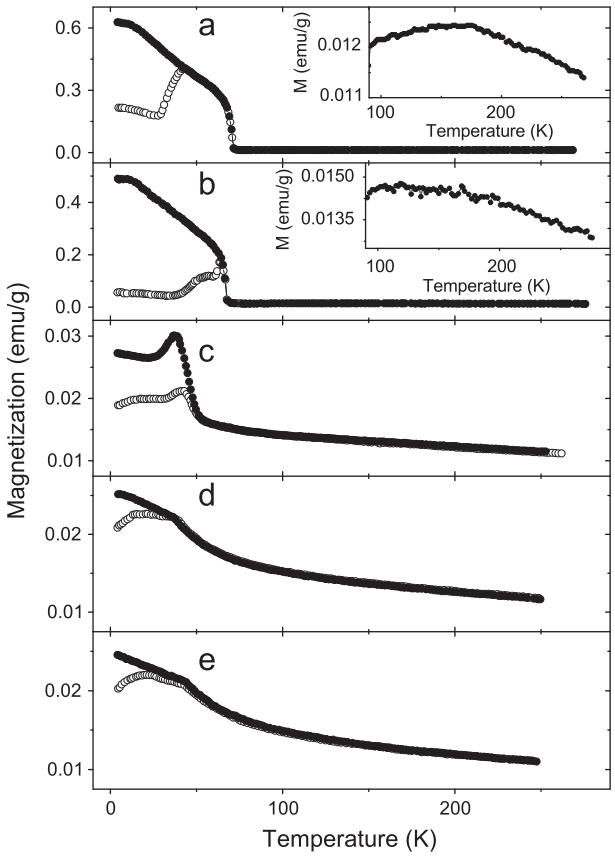

Fig. 5. Temperature dependences of magnetization of $Pb_3(Mn_{1-x}Fe_x)_7O_{15}$ in-plane applied field under the zero-field-cooled (open circle) and field-cooled (close circle) conditions ($H=500$ Oe). Inset shows the same curves enlarged. (a) x = 0, (b) x = 0.05 (c) x = 0.1, (d) x = 0.15 and (e) x = 0.2.

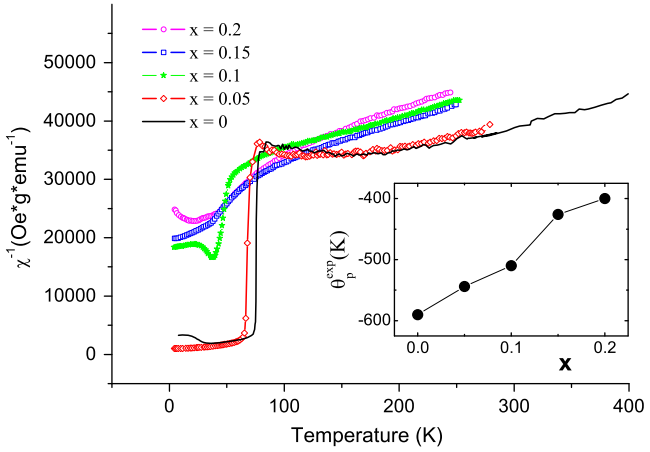

Fig. 6. Temperature dependences of inverse magnetic susceptibility χ^{-1} for $Pb_3(Mn_{1-x}Fe_x)_7O_{15}$. The inset shows the concentration dependence of the paramagnetic Curie temperature.

Fig. 6 demonstrates the temperature dependence of inverse magnetic susceptibility χ^{-1} for all the samples. It can be seen that above $T\sim200$ K the dependence is linear, i. e., is described by the Curie–Weiss law with paramagnetic Curie temperature θ_p^{exp} depending on iron content in the samples. The inset in Fig. 6 shows the dependence of θ_p^{exp} on *x* concentration of Fe^{3+} ions. The general trend to a decrease in the absolute value of θ with increasing iron content is observed. In addition, with increasing *x*, the linear portion of the dependence of χ^{-1} finishes at lower temperatures.

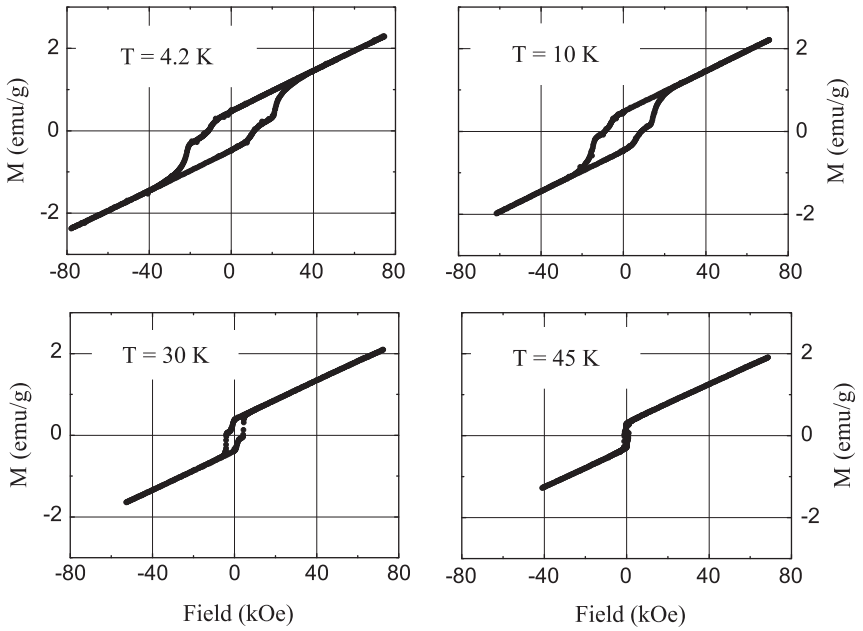

Fig. 7. Field dependences of magnetization for $Pb_3Mn_7O_{15}$ in the "in-plane" orientation of a magnetic field.

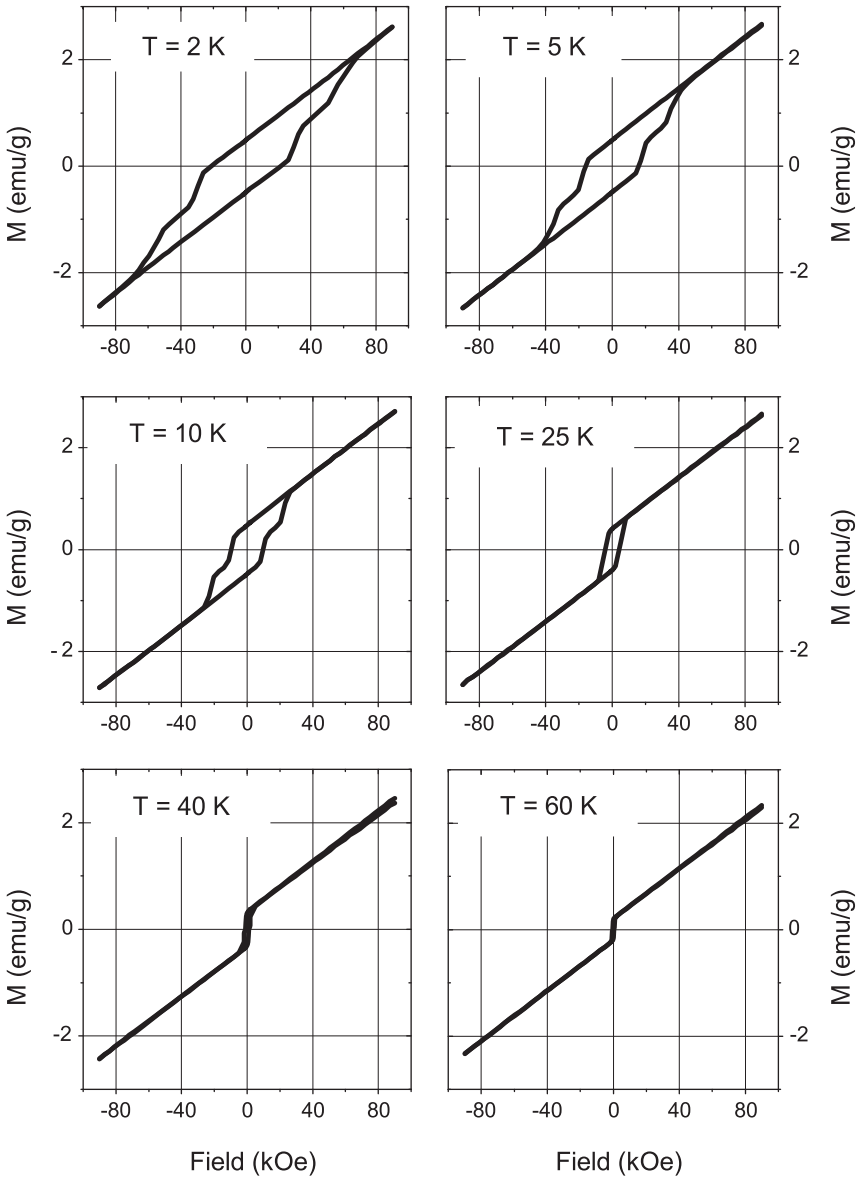

Fig. 8. Field dependences of magnetization for $Pb_3(Mn_{1-x}Fe_x)_7O_{15}$ with $x=0.05$ in the "in-plane" orientation of a magnetic field.

We measured field dependences of magnetization at different temperatures for all values of x. At $x=0$, the isothermal magnetization curves for $Pb_3Mn_7O_{15}$ obtained in the "in-plane" and "along-axis" magnetic fields below T_N show that the direction of the magnetic moment lies in the b–c plane (Fig. 7). With decreasing temperature, the value of this moment grows attaining 0.6 emu/g in an "in-plane" field of 500 Oe (Fig. 5a). In Fig. 7, one can see the hysteresis curves for the "in-plane" direction of a magnetic field with a coercive force of ~20 kOe at $T=4.2$ K. The hysteresis vanishes at $T=70$ K. Up to 80 kOe, no trend to saturation is observed at any temperatures. For the "along-axis" direction of a magnetic field, there is no hysteresis and the field dependence of magnetization is linear.

The samples with $x=0.05$ reveal very similar hysteresis loops (Fig. 8); the Neel temperature slightly decreases ($T_N=68$ K) as compared to that of the samples with $x=0$. We can say that small doping had the same effect as diamagnetic dilution accompanied, as a rule, by reduction of the transition temperature and the magnetization value. At $T=4.2$ K and $H=500$ Oe, the maximum magnetization values are $\sigma=0.6$ emu/g at $x=0$ and $\sigma=0.5$ emu/g at $x=0.05$.

In the samples with $x\geq0.1$, there is no hysteresis in the form observed in the samples with $x=0$ and $x=0.05$. Fig. 9 shows field dependences of magnetization for the sample with $x=0.1$ obtained at different temperatures. The remainder of the hysteresis is observed up to $T=25$ K. Magnetization measured in the field $H=500$ Oe decreases by more than an order of magnitude as compared to that of the nominally pure $Pb_3Mn_7O_{15}$ samples. At $T=40$ K, the hysteresis is not revealed at all; the field dependence of magnetization is linear, which is typical of paramagnets and antiferromagnets.

In the samples with $x=0.15$ and $x=0.2$, the considered hysteresis vanishes at all temperatures. Fig. 10 shows the isotherms for the sample with $x=0.15$ obtained at different temperatures from $T=2$ K to $T=40$ K. All the dependences have the same slope and the same magnetization value; at low temperatures, the dependences measured in increasing and decreasing magnetic field do not coincide. It is noteworthy that the magnetization curves for $x=0.15$ and $x=0.2$ are nearly identical at appropriate temperatures.

Note that, while in the pure sample and in the samples with $x=0$ and $x=0.05$ the hysteresis phenomena are observed only in the in-plane magnetic field, in the samples with $x\geq0.1$ the field dependences have the same form regardless of direction of the applied magnetic field, i. e., the magnetic characteristics of these samples are isotropic.

We attempted to explain such a surprising result, when substitution of a magnetic ion for a magnetic ion leads to the break of the long-range magnetic order in the system, by the following suggestions. As was established, the $Pb_3Mn_7O_{15}$ crystal has the pronounced layered structure; all manganese ions are in the octahedral surrounding of oxygen ions and nominally pure $Pb_3Mn_7O_{15}$ has nine nonequivalent positions of Mn ions at temperatures below 400 K. Taking into account that the paramagnetic Curie temperature of $Pb_3Mn_7O_{15}$ is $\theta=-590$ K and the temperature of the three-dimensional magnetic ordering is $T_N=72$ K, it is obvious that the magnetic structure is susceptible to strong geometrical frustrations [19]. In view of this, the magnetic structure is very complex and described neither as a classical two-sublattice antiferromagnet nor as a classical two-

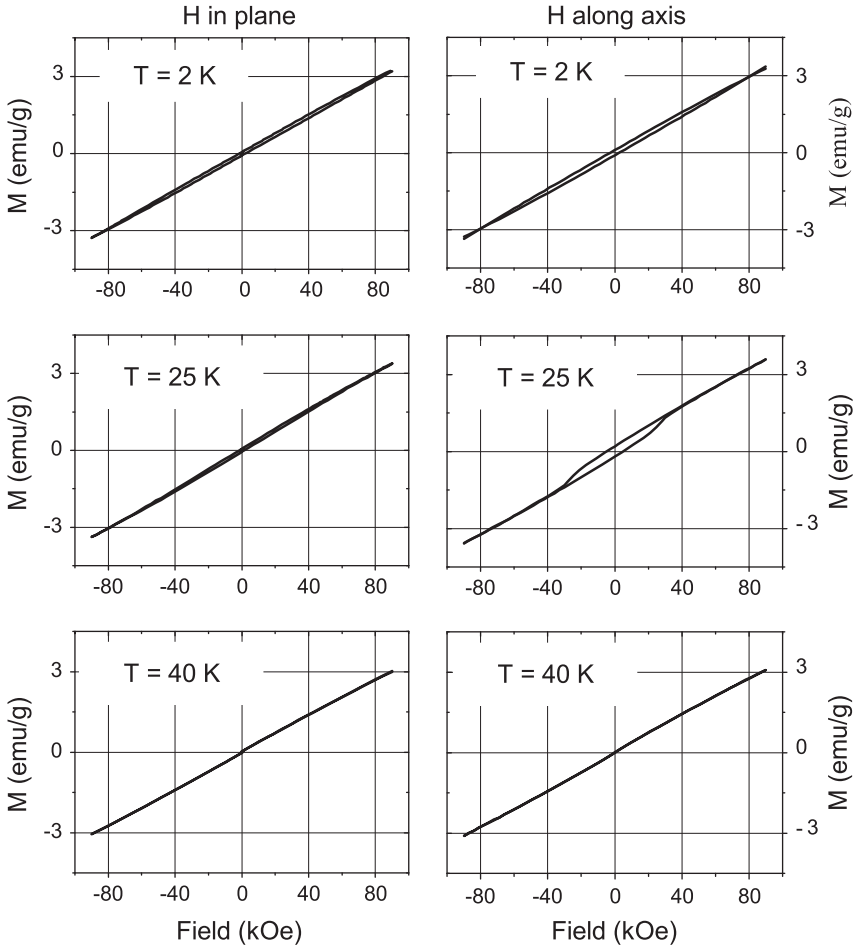

Fig. 9. Field dependences of magnetization of $Pb_3(Mn_{1-x}Fe_x)_7O_{15}$ with $x=0.1$ in the "in-plane" and "along-axis" orientation of magnetic field.

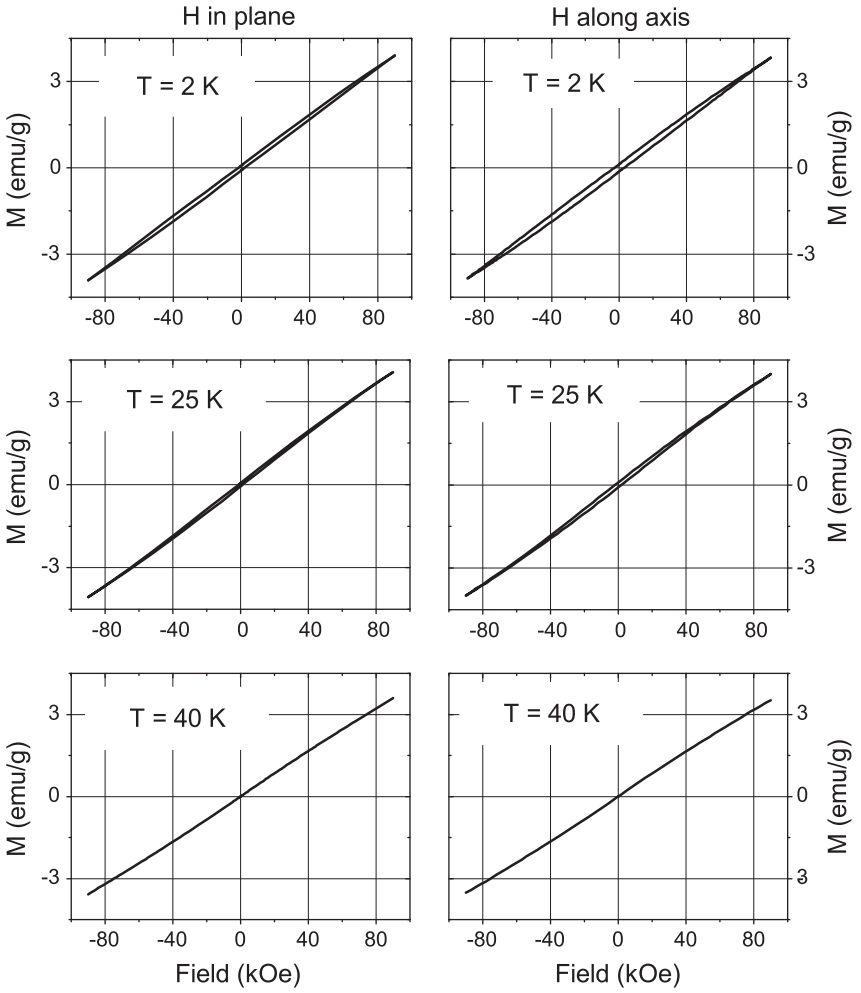

Fig. 10. Field dependences of magnetization of $Pb_3(Mn_{1-x}Fe_x)_7O_{15}$ with $x=0.15$ in the "in-plane" and "along-axis" orientation of magnetic field.

sublattice ferrimagnet. Most likely, there is the complex (possibly, triangular Kagome-type) magnetic ordering in the *b–c* (P_{nma}) planes. The magnetically ordered planes are coupled by the magnetic interaction implemented via columns consisting of two manganese ions Mn^{3+}–Mn^{3+}. In study [20], it was established using an empirical bond-valence-sum method that the positions in the columns are fully occupied by Mn^{3+} ions, which is quite natural, since these ions are Jahn–Teller and tend to strong distortions of the octahedral surrounding. It follows from the X-ray data that the oxygen octahedron is distorted the most just in the columns.

Upon substitution of iron ions for manganese ones in $Pb_3(Mn_{1-x}Fe_x)_7O_{15}$, a part of Fe^{3+} ions pass to the Fe2(8h) positions (in the hexagonal arrangement, $P6_3/mcm$). As a result, due to the competition of the exchange interactions, the geometry of the interplanar exchange implemented via the Fe^{3+}–Mn^{3+} columns can change. At the doping level $x > 0.1$, the three-dimensional ordering is apparently completely broken and the magnetic behavior of the system acquires the spin-glass-like character.

4. Conclusions

The $Pb_3(Mn_{1-x}Fe_x)_7O_{15}$ single crystals with $x=0$, 0.05, 0.1, 0.15, and 0.2 were grown by spontaneous crystallization from solution in melt. The XRD investigations have shown that all the $Pb_3Mn_7O_{15}$ single crystals doped with iron ions belong to the hexagonal space group $P6_3/mcm$. The XRD structure analysis and the Mossbauer data consistently indicate that iron ions enter the compound in the trivalent Fe^{3+} state and that the Mn2(8h) and Mn3(6f) sites in the structure are predominantly substituted by Fe.

The magnetic properties of $Pb_3(Mn_{1-x}Fe_x)_7O_{15}$ strongly depend on the doping level. At the low doping level ($x=0.05$), the temperature dependence of magnetization does not qualitatively change. There are only a minor decrease in magnetization, as compared to $Pb_3Mn_7O_{15}$, at the same external magnetic field and reduction of the Neel temperature T_N. The form of the field dependences of magnetization is nearly invariable. The situation becomes absolutely different starting from $x=0.1$. The broad peak at $T_1=160$ K vanishes, the long-range magnetic order does not occur, and the temperature dependences of magnetization at $x\geq 0.1$ exhibit the spin-glass-like features at low temperatures, with characteristic divergence of magnetization at different regimes of sample cooling (with and without magnetic field). In the samples with $x\geq 0.1$, the hysteresis in the form observed at $x=0$ and $x=0.05$ is absent. Unlike the samples with $x=0$ and $x=0.05$, in which the hysteresis phenomena are observed only for the magnetic field directed in the plane, in the samples with $x\geq 0.1$ the field dependences have the same form regardless of direction of the applied magnetic field; in other words, in these samples, the magnetic characteristics are isotropic.

Acknowledgments

The study was supported by the Ministry of Education and Science of Russian Federation, Project no. 8365 by the Siberian

Branch of the Russian Academy of Sciences, integration Project nos. 29 and 2.5.2.

References

[1] K.H. Kim, M. Uehara, V. Kiryukhin, S.W. Cheong, in: T. Chatterji (Ed.), Colossal Magnetoresistive Manganites, Kluwer–Academic, Dordrecht, 2004.
[2] N. Henry, L. Burylo-Dhuime, F. Abraham, O. Mentre, Physical Inorganic Chemistry 4 (2002) 1023.
[3] K. Wakiya, H. Sato, A. Miyazaki, T. Enoki, M. Isobe, Y. Ueda, Journal of Alloys and Compounds 317–318 (2001) 115.
[4] D. Holstam, B. Lindqvist, M. Johnsson, R. Norrestam, Canadian Mineral 29 (1991) 347–354.
[5] A.A. Bush, A.V. Titov, B.I. Al'shin, Yu.N. Venevtsev, Russian Journal of Inorganic Chemistry 22 (1977) 1211.
[6] N.V. Volkov, K.A. Sablina, O.A. Bayukov, E.V. Eremin, G.A. Petrakovskii, D. A. Velikanov, A.D. Balaev, A.F. Bovina, P. Boni, E. Clementyev, Journal of Physics: Condensed Matter 20 (2008) 055217.
[7] N.V. Volkov, E.V. Eremin, K.A. Sablina, N.V. Sapronova, Journal of Physics: Condensed Matter 22 (2010) 375901.
[8] N.V. Volkov, K.A. Sablina, E.V. Eremin, P. Böni, V.R. Shah, I.N. Flerov, A. Kartashev, J.C.E. Rasch, M. Boehm, J. Schefer, Journal of Physics: Condensed Matter 20 (2008) 445214.
[9] P.B. Darriet, M. Devalette, B. Latourrette, Acta Crystallographica B 34 (1978) 3528.
[10] R.E. Marsh, F.H. Herbstein, Acta Crystallographica B 39 (1983) 280.
[11] Y. Le Page, L.D. Calvert, Acta Crystallographica C 40 (1984) 1787.
[12] J.C.E. Rash, D.V. Sheptyakov, J. Schefer, L. Keller, M. Boehm, F. Gozzo, N. V. Volkov, K.A. Sablina, G.A. Petrakovskii, H. Grimmer, K. Conder, J.F. Loffler, Journal of Solution Chemistry 182 (2009) 1188.
[13] N.V. Volkov, L.A. Solovyov, E.V. Eremin, K.A. Sablina, S.V. Misjul, M.S. Molokeev, A.I. Zaitsev, M.V. Gorev, A.F. Bovina, N.V. Mihashenok, Physica B 407 (2012) 689.
[14] T.I. Milenov, P.M. Rafailov, V. Tomov, R.P. Nikolova, V. Skumryev, J.M. Igartua, G. Madariaga, E. G A L´opez, Iturbe-Zabalo, M.M. Gospodinov, Journal of Physics: Condensed Matter 23 (2011) 156001.
[15] J.M. Barandiaran, F.J. Bermejo, J. Gutierrez, L. Fernandez Barquin, Journal of Non-Crystalline Solids 353 (2007) 757.
[16] T.S. Zhao, W.X. Xianyu, B.H. Li, Z.N. Qian, Journal of Alloys and Compounds 459 (2008) 29.
[17] H.M. Rietveld, Journal of Applied Crystallography 2 (1969) 65.
[18] L.A. Solovyov, Journal of Applied Crystallography 37 (2004) 743.
[19] H. Kawamura, Journal of Physics: Condensed Matter 10 (1998) 4107.
[20] A.J.Kimber Simon, Journal of Physics: Condensed Matter 24 (2012) 186002.